ChemComm

COMMUNICATION

View Article Online
View Journal | View Issue

Cite this: *Chem. Commun.*, 2024, **60**, 6504

Received 5th April 2024,
Accepted 29th May 2024

DOI: 10.1039/d4cc01568a

rsc.li/chemcomm

Selective monoborylation of methane by metal–organic framework confined mononuclear pyridylimine-iridium(I) hydride†

Rahul Kalita,[a] Manav Chauhan,[a] Poorvi Gupta,[a] Wahida Begum,[a] Chhaya Thadhani,[a] Biplab Ghosh,[b] Balendra,[a] Himani Bisht[a] and Kuntal Manna *[a]

Chemoselective monoborylation of methane in high yield is a grand challenge. We have developed a metal–organic framework confined pyridylimine-iridium hydride catalyst, which is efficient in methane C–H borylation using bis(pinacolato)diboron to afford methyl boronic acid pinacol ester in 98% GC-yield at 130 °C with a TON of 196. Mechanistic investigation suggests the oxidative addition of methane to $Ir^{III}(Bpin)_2(H)$ species to form $Ir^{V}(Bpin)_2(CH_3)(H)_2$ as the turnover limiting step.

Chemoselective C–H borylation of methane has drawn significant attention in recent years due to the abundance of methane as the low-cost carbon feedstock and the application of organoborane products as versatile synthetic intermediates in organic synthesis.[1–3] However, the methane C–H bond activation under mild conditions is highly challenging owing to the intrinsic inertness stemming from the considerable C–H bond dissociation energy (104 kcal mol^{-1}) with a large HOMO–LUMO gap, low acidity and polarization difficulty.[4–7] In addition, methane borylation reactions typically suffer from poor selectivity originating from the over-borylation of methane C–H bonds, competitive solvent C–H borylation, and boron-byproduct formation. Furthermore, the mono-functionalized product is more reactive than methane itself, making the selective monoborylation of methane extremely challenging.

Early reports of developing homogeneous catalysts for methane borylation using bis(pinacolato)diboron (B_2pin_2) as the borylating agent were based on 1,10-phenanthroline- and diphosphine-ligated Ir, Rh and Ru complexes, which gave a mixture of monoborylated (CH_3Bpin) and diborylated methane [$CH_2(Bpin)_2$] at 150 °C with selectivity spanning 2 : 1 to 31 : 1.[8,9] Farha and co-workers elegantly employed a metal–organic framework (MOF) as the porous solid support with appropriate pore sizes,[10–19] in which an embedded iridium(III) catalyst enables selective mono C–H borylation over multiborylation of methane within the confined reaction space *via* shape-selective catalysis, leading to the formation of CH_3Bpin in 19.5% yield with a turnover number (TON) of 67.[20] Subsequently, a mono(phosphine) MOF-supported-Ir catalyst outperformed other Ir-catalysts based on chelating phenanthroline, bipyridine, and diphosphine ligands to give CH_3Bpin with a TON of 127.[21] Despite significant progress in developing catalysts for selective monoborylation of methane, these catalytic systems also generate a considerable amount of boron-byproducts such as HOBpin, pinBOBpin and Sol-Bpin during the borylation reactions.[22–24] Herein, we report a MOF-confined mononuclear pyridylimine-ligated iridium(I)-hydride, which is a highly robust and active heterogeneous catalyst for chemoselective monoborylation of methane to afford CH_3Bpin in a near-quantitative yield (Fig. 1).

Pyrim-UiO-IrH MOF has a UiO-68 topology,[15,25] built from $Zr_6O_4(OH)_4$ nodes and linear 2′-amino-[1,1′:4′,1″-terphenyl]-4,4″-dicarboxylate bridging linkers bearing pyridylimine-ligated iridium(I)-hydride species. Pyrim-UiO-IrH was synthesized by metalation of a pyridylimine-functionalized zirconium UiO-68-MOF (pyrim-UiO) with $IrCl_3{\cdot}3H_2O$ followed by treatment of

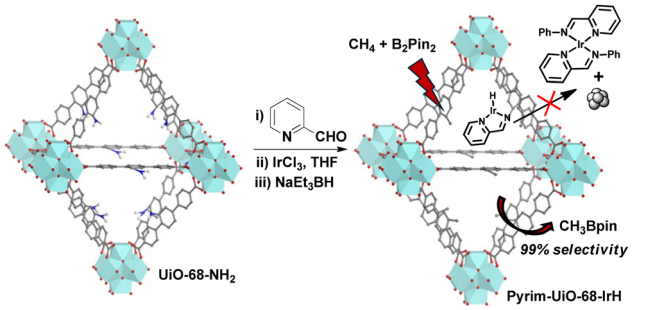

Fig. 1 Synthesis of pyrim-UiO-IrH MOF *via* post-synthetic modification of pristine amino-functionalized UiO-68-MOF for methane monoborylation.

[a] *Department of Chemistry, Indian Institute of Technology Delhi, Hauz Khas, New Delhi 110016, India. E-mail: kmanna@chemistry.iitd.ac.in*
[b] *BARC Beamlines Section, Indus-2, RRCAT, Indore 452013, India*

† Electronic supplementary information (ESI) available. See DOI: https://doi.org/10.1039/d4cc01568a

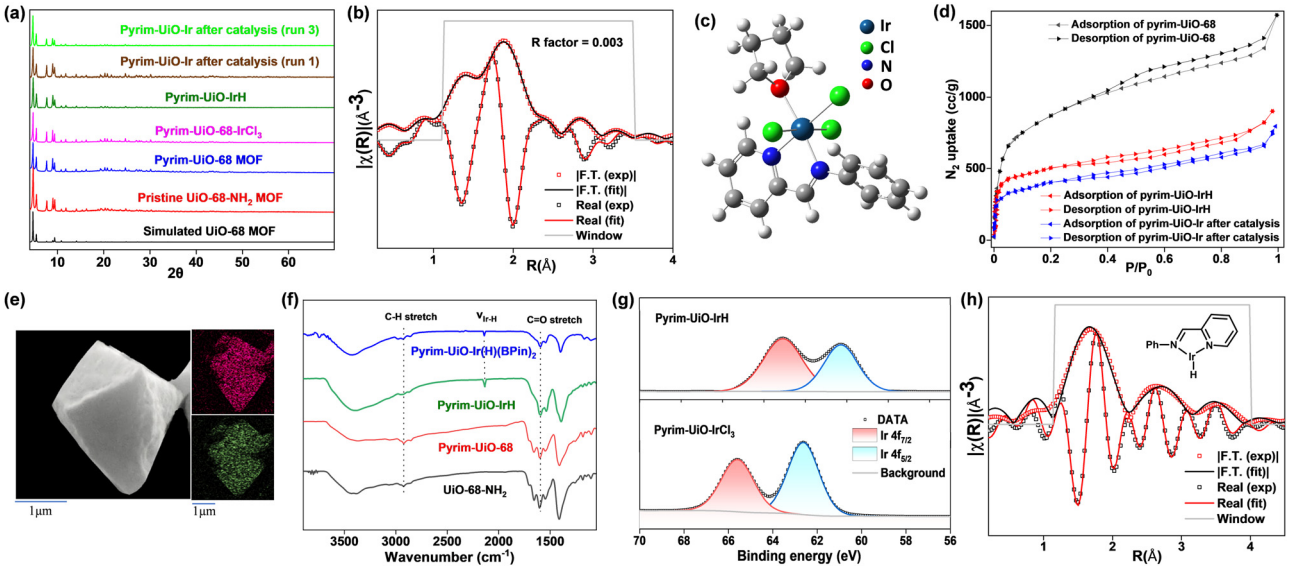

Fig. 2 (a) PXRD patterns of simulated UiO-68 MOF (black), pristine UiO-68-NH_2 MOF (red), pyrim-UiO-68 MOF (blue), pyrim-UiO-$IrCl_3$ (magenta), pyrim-UiO-IrH (olive), pyrim-UiO-Ir after run 1 (brown) and pyrim-UiO-Ir after run 3 (green). (b) EXAFS spectra (red and black hollow squares) and fits (red and black solid lines) of pyrim-UiO-$IrCl_3$ in the *R* space from 1.15–3.5 Å. (c) DFT optimised structure of (pyrim)$IrCl_3$(THF) molecule. (d) BET nitrogen sorption isotherms of pyrim-UiO-68 (black), pyrim-UiO-IrH (red) and pyrim-UiO-Ir after catalysis (blue) measured at 77 K. (e) SEM image of a pyrim-UiO-IrH particle along with elemental mapping of Zr and Ir. (f) IR (KBr) spectrum of UiO-68-NH_2 (black), pyrim-UiO-68 MOF (red), pyrim-UiO-IrH (green) and pyrim-UiO-IrH($BPin)_2$ (blue). (g) Ir 4f XPS spectra of pyrim-UiO-$IrCl_3$ and pyrim-UiO-IrH. (h) EXAFS spectra (red and black hollow squares) and fits (red and black solid lines) of pyrim-UiO-IrH in the *R* space from 1.15–4.0 Å.

$NaEt_3BH$.[26] The reaction of pyrim-UiO MOF and $IrCl_3{\cdot}3H_2O$ in THF formed pyrim-UiO-$IrCl_3$ MOF bearing pyridylimine-ligated $IrCl_3$ species at its linkers. The extended X-ray absorption fine structure (EXAFS) of pyrim-UiO-$IrCl_3$ at the Ir L_3-edge fitted well with the DFT-optimized structure of (pyrim)$IrCl_3$(THF), indicating the presence of an octahedral Ir^{III}-species, in which Ir^{3+} ion is coordinated two nitrogen atoms of pyridylimine, three chlorine atoms and a THF molecule (Fig. 2b). The treatment of pyrim-UiO-$IrCl_3$ with $NaEt_3BH$ in THF at room temperature furnished pyrim-UiO-IrH. PXRD patterns of pyrim-UiO-IrH, simulated UiO-68 MOF, and pristine UiO-68-NH_2 are comparable indicating that pyrim-UiO-IrH has a UiO-68 topology and that pristine MOF's structure and crystallinity were not altered during post-synthetic modifications (Fig. 2a).

Inductively coupled plasma-optical emission spectroscopy (ICP-OES) analysis of the digested pyrim-UiO-IrH revealed a Ir-loading of ~32% with respect to the pyridylimine moiety, corresponding to the formula of $Zr_6(\mu_3\text{-}O)_4(\mu_3\text{-}OH)_4(C_{26}H_{16}N_2O_4Ir_{0.32}\text{-}H_{0.32})_6$. Pyrim-UiO-IrH has a BET surface area of 1245 $m^2\ g^{-1}$, and a pore size of 0.8 nm, which is lower than that of pristine pyrim-UiO MOF, due to the incorporation of iridium-moiety within the MOF's pores (Fig. 2d). Scanning electron microscopy-energy

Table 1 Optimization of pyrim-UiO-IrH catalyzed mono C–H borylation of methane[a]

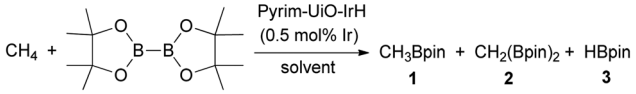

Entry	Solvent	*T* (°C)	*P* (bar)	Time (h)	Conv. of B_2pin_2	%Yield of 1[b] (selectivity)[c]	TON
1	C_6H_{12}	130	40	24	100	98 (98)	196
2	THF	130	40	24	89	29 (33)	58
3	Toluene	130	40	24	80	35 (44)	70
4	Heptane	130	40	24	84	72 (86)	144
5	C_6H_{12}	130	40	18	87	85 (98)	170
6	C_6H_{12}	110	40	24	20	19 (95)	38
7	C_6H_{12}	150	40	24	100	78 (78)	156
8	C_6H_{12}	130	20	24	27	26 (96)	52
9	C_6H_{12}	130	30	24	48	47 (98)	94
10	C_6H_{12}	130	40	48	100	82 (82)	164

[a] Reaction conditions: 1.9 mg of pyrim-UiO-IrH (1.02 μmol of Ir), 51 mg B_2pin_2 (0.2 mmol), 2 mL solvents. [b] Yield was determined by GC as GC peak area (CH_3Bpin)/peak area (total boron species) × 100. [c] Selectivity was calculated as GC peak area (CH_3Bpin)/peak area (total products) × 100.

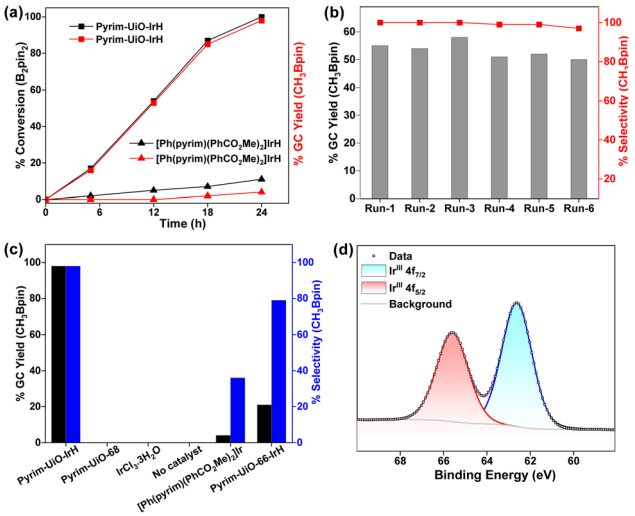

Fig. 3 (a) Plot of %GC conversion and %GC yield of CH_3Bpin vs time for CH_4 borylation using pyrim-UiO-IrH (0.5 mol% Ir) and [Ph(pyrim)$(PhCO_2Me)_2$]IrH (0.5 mol% Ir) under identical conditions. (b) Plot for the %GC yield and %selectivity of CH_3Bpin at various runs in the recycling of pyrim-UiO-IrH (0.5 mol% Ir). (c) Comparison of the catalytic activity for the conversion of CH_4 to CH_3Bpin over pyrim-UiO-IrH with other catalysts under identical reaction conditions. Conditions: 1.9 mg of pyrim-UiO-IrH (1.02 μmol of Ir) or equivalent Ir-loading for other catalysts, 2 mL C_6H_{12}, 130 °C, 40 bar CH_4 and 24 h. (d) Ir 4f XPS spectrum of pyrim-UiO-IrH$(Bpin)_2$.

dispersive X-ray analysis (SEM-EDX) mapping of pyrim-UiO-IrH displayed uniform distributions of Ir and Zr ions through the MOF particle (Fig. 2e). The IR spectrum (KBr) of pyrim-UiO-IrH showed a characteristic ν_{Ir-H} stretching frequency at 2140 cm^{-1} (Fig. 2f). X-ray absorption near edge structure (XANES) showed the Ir L_3-edge energy of pyrim-UiO-IrH at 11.216 KeV, which is 3 eV lower than that of pyrim-UiO-$IrCl_3$ and 1.0 eV higher than Ir(0) foil, suggesting a formal +1 oxidation state for Ir ion in pyrim-UiO-IrH (Fig. S18, ESI†). The existence of Ir^I-species in pyrim-UiO-IrH was further confirmed by X-ray photoelectron spectroscopy (XPS), which displayed Ir $4f_{7/2}$ and $4f_{5/2}$ binding energy peaks at 60.3 eV and 63.1 eV, respectively, and ~2.1–2.3 eV lower than those of pyrim-UiO-$IrCl_3$ and $IrCl_3$ (Fig. 2g). The EXAFS analysis of pyrim-UiO-IrH at the Ir L_3-edge suggests the existence of mono pyridylimine-ligated iridium(I)-hydride moiety within the MOF (Fig. 2h).

Pyrim-UiO-IrH catalyzed methane borylation reactions were conducted in a high-pressure batch reactor using B_2pin_2 as the borylating agent and the limiting reagent in a suitable solvent under a desired methane pressure. Initial trials using 0.2 mmol of B_2pin_2 and pyrim-UiO-IrH (0.5 mol% Ir) in several different solvents at 130 °C under 40 bar of CH_4 for 24 h revealed that cyclohexane gave the highest yield of CH_3Bpin (98%) with complete conversion of B_2pin_2 (entries 1–4, Table 1). CH_4 borylation in other solvents such as THF, toluene, heptane and DMF gave lesser yields of CH_3Bpin, due to the formation of various byproducts such as borylated solvents, $CH_2(Bpin)_2$, pinBOBpin, and HOBpin.[20] Further screening of reaction temperature, CH_4 pressure, catalyst loading, and reaction time showed that 0.5 mol% Ir- loading, 130 °C, 40 bar of CH_4, and 24 h of reaction are optimal for selective mono-borylation of methane (entry 1, Table 1). The borylation reaction did not occur below 100 °C, however, the formation of a significant amount of HOBpin, pinBOBpin and $C_6H_{11}Bpin$ was observed at 150 °C (entries 6 and 7, Table 1). The borylation reactions under 20 bar and 30 bar of CH_4 afforded CH_3Bpin in only 26% and 47% yields, respectively (entries 8 and 9, Table 1), presumably due to the lower solubility of CH_4 at lower pressure. Pyrim-UiO-IrH catalyzed CH_4 borylation under optimal reaction conditions afford CH_3Bpin in 98% yield, giving rise to the highest TON of 196 (entry 1, Table 1). Gas chromatography (GC) analysis of the crude reaction mixture showed the exclusive formation of CH_3Bpin with no detectable diborylated product $CH_2(Bpin)_2$.

Importantly, pyrim-UiO-IrH was at least 24 times more active than its homogeneous control ([Ph(pyrim)$(PhCO_2Me)_2$]IrH, which produced only 4% CH_3Bpin under the identical reaction conditions and Ir-loading (0.5 mol%) (Fig. 3a). The much higher catalytic activity of pyrim-UiO-IrH than its homogeneous Ir analogue is likely due to the greater stability of the pyrim-IrH species *via* active-site isolation at the linkers that prevent intermolecular decomposition.

As a heterogeneous catalyst, pyrim-UiO-Ir could be recycled and reused at least 5 times with consistent activity without noticeable changes in structure or crystallinity, leading to the total TON up to 980 (Fig. 3b). No borylated product was detected when the methane borylation was carried out in the absence of MOF catalyst or with the pristine pyrim-UiO-68 or

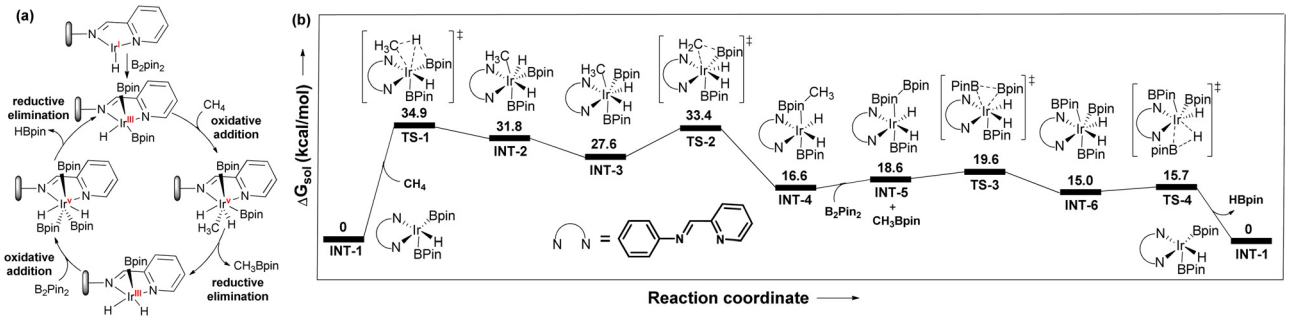

Fig. 4 (a) Proposed catalytic cycle of pyrim-UiO-IrH catalyzed methane borylation. (b) DFT-calculated free energy profile at 403 K for pyrim-UiO-IrH catalyzed methane borylation reaction.

with $IrCl_3{\cdot}3H_2O$ (entries 15–17, Table S1, ESI†). The production of CH_3Bpin ceased upon removing the solid MOF pyrim-UiO-IrH from the reaction mixture, suggesting that the catalytic moiety is embedded within the MOF (Fig. S6, ESI†). A catalytic reaction with 40 bar N_2 instead of CH_4 and 0.2 mmol B_2Pin_2 was conducted at 130 °C in cyclohexane for 24 h. In this reaction, no CH_3Bpin product was formed, signifying CH_4 as the only carbon source for CH_3Bpin formation (Section S4.2, ESI†). Importantly, pyrim-UiO-68-IrH was almost four times more active and significantly chemoselective than pyrim-UiO-66-IrH MOF, having similar UiO-topology but smaller pore sizes in methane borylation due to the facile diffusion of the substrates and formation of smaller monoborylated products within the pores of UiO-68 MOFs *via* shape-selective catalysis (Fig. S10 and Section S4.5.2, ESI†).

The reaction between pyrim-UiO-$Ir^{I}H$ and B_2Pin_2 at 130 °C for 30 min forms pyrim-UiO-$Ir^{III}(Bpin)_2(H)$, which was characterized by XPS and IR spectroscopy (Fig. 2f and 3d). Pyrim-UiO-$Ir^{III}(Bpin)_2(H)$ showed similar catalytic activity to pyrim-UiO-68-$Ir^{I}H$, suggesting $Ir^{III}(Bpin)_2(H)$ species as the potential catalytic intermediate. We propose that pyrim-UiO-Ir catalyzed methane borylation proceeds *via* a Ir^{III}–Ir^{V}–Ir^{III} catalytic cycle,[20,22] in which the oxidative addition of methane to pyrim-UiO-$Ir^{III}(Bpin)_2(H)$ (INT-1) first form seven coordinated pyrim-UiO-$Ir^{V}(CH_3)(H)_2(Bpin)_2$ (INT-2) followed by reductive elimination of CH_3Bpin to generate pyrim-UiO-$Ir^{III}(Bpin)(H)_2$ (Fig. 4). Further oxidative addition of B_2Pin_2 followed by reductive elimination of HBpin regenerates pyrim-UiO-$Ir^{III}(Bpin)_2(H)$. DFT calculation suggests that the boron-assisted oxidative addition of methane is the turn-over limiting step requiring a free activation energy of 34.9 kcal mol^{-1}, similar to the reported 1,10-phenanthroline- and diphosphine-ligated Ir catalysts.[20,22]

However, the higher catalytic activity of pyrim-UiO-Ir in methane borylation is attributed to the facile oxidative addition of methane to the $Ir^{III}(H)(Bpin)_2$ species as opposed to the sterically encumbered $Ir^{III}(Bpin)_3$ species in other systems. In conclusion, we have developed a porous MOF-supported iridium catalyst for chemoselective monoborylation of methane, affording CH_3Bpin in 98% yield, which is much higher than the previous reports. This work highlights the importance of MOFs in developing heterogeneous catalysts for chemoselective functionalization of methane and other hydrocarbons.

Conflicts of interest

There are no conflicts to declare.

Notes and references

1 J.-Y. Cho, M. K. Tse, D. Holmes, R. E. Maleczka and M. R. Smith, *Science*, 2002, **295**, 305–308.
2 T. Ishiyama, J. Takagi, J. F. Hartwig and N. Miyaura, *Angew. Chem., Int. Ed.*, 2002, **41**, 3056–3058.
3 I. A. I. Mkhalid, J. H. Barnard, T. B. Marder, J. M. Murphy and J. F. Hartwig, *Chem. Rev.*, 2010, **110**, 890–931.
4 S. J. Blanksby and G. B. Ellison, *Acc. Chem. Res.*, 2003, **36**, 255–263.
5 H. Schwarz, *Angew. Chem., Int. Ed.*, 2011, **50**, 10096–10115.
6 W. Taifan and J. Baltrusaitis, *Appl. Catal., B*, 2016, **198**, 525–547.
7 N. J. Gunsalus, A. Koppaka, S. H. Park, S. M. Bischof, B. G. Hashiguchi and R. A. Periana, *Chem. Rev.*, 2017, **117**, 8521–8573.
8 A. K. Cook, S. D. Schimler, A. J. Matzger and M. S. Sanford, *Science*, 2016, **351**, 1421–1424.
9 K. T. Smith, S. Berritt, M. González-Moreiras, S. Ahn, M. R. Smith, M.-H. Baik and D. J. Mindiola, *Science*, 2016, **351**, 1424–1427.
10 M. Eddaoudi, J. Kim, N. Rosi, D. Vodak, J. Wachter, M. O'Keeffe and O. M. Yaghi, *Science*, 2002, **295**, 469–472.
11 J. Lee, O. K. Farha, J. Roberts, K. A. Scheidt, S. T. Nguyen and J. T. Hupp, *Chem. Soc. Rev.*, 2009, **38**, 1450.
12 I. Senkovska, F. Hoffmann, M. Fröba, J. Getzschmann, W. Böhlmann and S. Kaskel, *Microporous Mesoporous Mater.*, 2009, **122**, 93–98.
13 H. Furukawa, K. E. Cordova, M. O'Keeffe and O. M. Yaghi, *Science*, 2013, **341**, 1230444.
14 C. Wang, D. Liu and W. Lin, *J. Am. Chem. Soc.*, 2013, **135**, 13222–13234.
15 Y. Bai, Y. Dou, L.-H. Xie, W. Rutledge, J.-R. Li and H.-C. Zhou, *Chem. Soc. Rev.*, 2016, **45**, 2327–2367.
16 M. Rimoldi, A. J. Howarth, M. R. DeStefano, L. Lin, S. Goswami, P. Li, J. T. Hupp and O. K. Farha, *ACS Catal.*, 2017, **7**, 997–1014.
17 M. Kalaj and S. M. Cohen, *ACS Cent. Sci.*, 2020, **6**, 1046–1057.
18 B. Pramanik, R. Sahoo and M. C. Das, *Coord. Chem. Rev.*, 2023, **493**, 215301.
19 G. Cai, P. Yan, L. Zhang, H. C. Zhou and H. L. Jiang, *Chem. Rev.*, 2021, **121**, 12278–12326.
20 X. Zhang, Z. Huang, M. Ferrandon, D. Yang, L. Robison, P. Li, T. C. Wang, M. Delferro and O. K. Farha, *Nat. Catal.*, 2018, **1**, 356–362.
21 X. Feng, Y. Song, Z. Li, M. Kaufmann, Y. Pi, J. S. Chen, Z. Xu, Z. Li, C. Wang and W. Lin, *J. Am. Chem. Soc.*, 2019, **141**, 11196–11203.
22 S. Ahn, D. Sorsche, S. Berritt, M. R. Gau, D. J. Mindiola and M.-H. Baik, *ACS Catal.*, 2018, **8**, 10021–10031.
23 Q. Chen, A. Dong, D. Wang, L. Qiu, C. Ma, Y. Yuan, Y. Zhao, N. Jia, Z. Guo and N. Wang, *Angew. Chem.*, 2019, **131**, 10781–10786.
24 O. Staples, M. S. Ferrandon, G. P. Laurent, U. Kanbur, A. J. Kropf, M. R. Gau, P. J. Carroll, K. McCullough, D. Sorsche, F. A. Perras, M. Delferro, D. M. Kaphan and D. J. Mindiola, *J. Am. Chem. Soc.*, 2023, **145**, 7992–8000.
25 H. Cavka, S. Jakobsen, U. Olsbye, N. Guillou, C. Lamberti, S. Bordiga and K. P. Lillerud, *J. Am. Chem. Soc.*, 2008, **130**, 13850–13851.
26 R. Newar, W. Begum, N. Antil, S. Shukla, A. Kumar, N. Akhtar, Balendra and K. Manna, *Inorg. Chem.*, 2020, **59**, 10473–10481.